Journal of Power Sources 192 (2009) 208–215

Contents lists available at ScienceDirect

Journal of Power Sources

journal homepage: www.elsevier.com/locate/jpowsour

Dynamic modeling of a three-stage low-temperature ethanol reformer for fuel cell application

Vanesa M. García [a,*], Eduardo López [b], Maria Serra [a], Jordi Llorca [b]

[a] Institut de Robòtica i Informàtica Industrial (CSIC-UPC), Llorens i Artigas 4-6, 08028 Barcelona, Spain
[b] Institut de Tècniques Energètiques, Universitat Politècnica de Catalunya, Diagonal 647, ed. ETSEIB, 08028 Barcelona, Spain

ARTICLE INFO

Article history:
Received 15 October 2008
Received in revised form 12 December 2008
Accepted 15 December 2008
Available online 24 December 2008

Keywords:
Hydrogen production
Ethanol steam reforming
Low-temperature reforming
Dynamic simulation

ABSTRACT

A low-temperature ethanol reformer based on a cobalt catalyst for the production of hydrogen has been designed aiming the feed of a fuel cell for an autonomous low-scale power production unit. The reformer comprises three stages: ethanol dehydrogenation to acetaldehyde and hydrogen over SnO_2 followed by acetaldehyde steam reforming over Co(Fe)/ZnO catalyst and water gas shift reaction. Kinetic data have been obtained under different experimental conditions and a dynamic model has been developed for a tubular reformer loaded with catalytic monoliths for the production of the hydrogen required to feed a 1 kW PEMFC.

1. Introduction

Fuel cells are attractive power sources largely because they can achieve efficiencies much greater than conventional engines. However, among the most daunting challenges limiting the implementation of fuel cells is the development of a sustainable source of hydrogen. Ethanol is a promising source of hydrogen as it is a renewable source when obtained from biomass, and hence, catalytic steam reforming of ethanol to produce hydrogen for fuel cells is acquiring increasing interest (Eq. (1)). The reaction has been extensively studied over catalysts based on Ni, Ni/Cu, Co, and noble metals (Pd, Pt, Rh and Ru) [1,2]. The reaction is highly endothermic $\Delta H_{298}{}^{\circ} = 347.4\,\text{kJ mol}^{-1}$, which accounts for the requirement of reforming temperatures usually above 873 K. At such high temperatures ethanol is mainly reformed into a mixture of H_2 and CO (Eq. (2)), and it is necessary to pass the reformate through a water gas shift reactor in order to generate further hydrogen and eliminate CO (Eq. (3)), which is a strong fuel cell poison. However, cobalt-based catalysts are particularly effective for ethanol steam reforming at lower temperature, 623–673 K [3–6], where the water gas shift reaction is also operative. For this reason, increasing attention is being focused on developing low-temperature catalytic processes with cobalt catalysts.

$$C_2H_5OH + 3H_2O \rightarrow 6H_2 + 2CO_2 \quad (1)$$

$$C_2H_5OH + H_2O \rightarrow 4H_2 + 2CO \quad (2)$$

$$CO + H_2O \rightarrow +CO_2 + H_2 \quad (3)$$

Among different supported cobalt catalysts already tested for low-temperature ethanol steam reforming, the best performance in terms of hydrogen generation, CO_2/CO ratio, and long-term stability is ZnO-supported cobalt [3]. At 673 K, 5.3–5.4 mol H_2 per mol of reacted ethanol is obtained and almost no CO is present in the reformate when a bioethanol-like mixture (C_2H_5OH:H_2O~13 mol) is reacted at 5000 h^{-1} [4]. The main undesired product obtained over Co/ZnO is methane (<3% on a dry basis). Methane may be formed during ethanol steam reforming by ethanol decomposition (Eq. (4)) or methanation of CO or CO_2 (Eq. (5)):

$$C_2H_5OH \rightarrow H_2 + CH_4 + CO \quad (4)$$

$$CO_n + (2+n)H_2 \rightarrow CH_4 + nH_2O \quad (5)$$

Methanation is a very costly side reaction for the production of hydrogen because it consumes between 3 and 4 mol of hydrogen for each mol of methane formed. In addition, the reaction is thermodynamically favored at low temperature. Following a survey addressed to improve the catalytic performance of the Co/ZnO system for real ethanol steam reforming application, it has been recently reported that the addition of iron has a positive effect in decreasing methane formation [7]. Under the same experimental conditions tested for Co/ZnO, a Co(Fe)/ZnO catalyst with a molar ratio of Co:Fe~10:1 yields up to 30 times less methane. The enrichment in iron that occurs on the surface of cobalt particles in Co(Fe)/ZnO as determined by X-ray photoelectron spectroscopy [7]

* Corresponding author. Tel.: +34 93 401 57 89.
E-mail address: vgarcia@iri.upc.edu (V.M. García).

0378-7753/$ – see front matter © 2008 Elsevier B.V. All rights reserved.
doi:10.1016/j.jpowsour.2008.12.055

Nomenclature

C	concentration (mol m_R^{-3})
c_p	specific heat (J kg^{-1} K^{-1})
d_t	monolith external diameter (m)
F_T	total molar flow (mol s^{-1})
k	reaction rate constant, STAGE 1 (mL g_{cat}^{-1} h^{-1})
k'	reaction rate constant, STAGE 2 (mL g_{cat}^{-1} h^{-1})
L	monolith length (m)
Q	volumetric flowrate at reactor inlet (mL min^{-1})
r	reaction rate (mol m_R^{-3} s^{-1})
t	time (s)
T	temperature (K)
T_F	furnace temperature (K)
U	overall heat-transfer coefficient (J s^{-1} m^{-2} K^{-1})
v	superficial velocity (m s^{-1})
W	catalyst mass (g)
x	conversion
y	molar fraction
z	axial coordinate (m)

Subscripts

cat	catalyst
g	gas
i	reaction number, $i = 1, \ldots, 3$ (Eqs. (6), (10) and (3), respectively)
in	at reactor inlet
j	component number, $j = 1, \ldots, 6$ (C_2H_5OH, H_2O, C_2H_4O, H_2, CO, CO_2, respectively)
out	at reactor outlet
R	reactor
s	solid

Greek letters

ΔH_{298}°	heat of reaction (J mol^{-1})
ε	bed void fraction ($(1 - m_s^3)\, m_R^3$)
ν_{ji}	stoichiometric coefficient of component j in reaction i
ρ	density (kg m^{-3})

is expected to modify the surface of cobalt particles and destroy methanation sites with respect to pure cobalt particles.

Another important issue of ethanol reforming is catalyst deactivation. Major deactivation by coking at high temperature (>873 K) has been reported to be severe over several catalysts [8]. The dehydration of ethanol to ethylene, catalyzed by acid sites on the support [9], is responsible for the formation of polyethylene on the catalyst surface, which in turn is converted to poorly organized graphitic carbon, or even nanotubes [10]. Deactivation by carbon deposition over Co/ZnO during ethanol steam reforming is strongly temperature-dependent, and only above 723 K it becomes severe [3]. However, the addition of Na^+ promoter in the preparation of Co/ZnO improves the stability of the catalyst by suppressing acid sites responsible for carbon deposition [11]. Therefore, ZnO-supported cobalt doped with iron and Na^+ appears to be an effective, stable, and low-cost catalyst for generating hydrogen for fuel cell application through ethanol steam reforming at low temperature.

A critical point encountered when ethanol steam reforming is carried out over cobalt-based catalysts (and probably over other supported metals as well) is that the active site for the reforming reaction involves cobalt in a metallic state, but metallic cobalt is formed on the catalyst surface only when the production of hydrogen has started because, initially, the reactants (ethanol and excess water) oxidize the surface of cobalt particles. This has been demonstrated to occur by detailed characterization studies carried out with *in situ* infrared spectroscopy [12] and *in situ* magnetic measurements under real operation conditions [13]. The answer to this apparent contradiction comes from mechanistic studies. The first step of the low-temperature ethanol steam reforming pathway over cobalt is ethanol dehydrogenation over cobalt oxide to yield equal amounts of acetaldehyde and hydrogen (Eq. (6)) [14]. Then, the hydrogen produced in this first step reduces cobalt oxide into metallic cobalt and the second step of the reaction occurs, which is the reforming of acetaldehyde with steam over metallic cobalt [14].

The need for a reducing atmosphere for the reforming step of the process makes ethanol steam reforming over cobalt highly dependent on reaction conditions. One possibility for maintaining a reducing atmosphere over the cobalt catalyst and overcome the problem could be by separating the two steps of the overall reaction in two catalytic beds and by using two different catalysts: a first step where ethanol dehydrogenates into acetaldehyde and hydrogen over an appropriate catalyst, followed by the reforming of acetaldehyde over the cobalt catalyst. In this way, the cobalt catalyst would be always under hydrogen atmosphere resulting from ethanol dehydrogenation in the first step, and not influenced by variations in the redox environment given by reactants and products during the reforming step. An additional advantage of this method is that it allows maintaining a different temperature regime for each step of the reaction, which may result in a better thermal optimization of the process, which in turn may benefit the final selectivity of the process towards the reforming products, H_2 and CO_2. Finally, to lower down the CO content, a water gas shift module operating at a lower temperature can be introduced as third step. In Fig. 1, a schematic draw of the three stages reforming process is shown.

In this work we address the dynamic modeling of such a three-module device for feeding hydrogen to a fuel cell. We have chosen three specific catalysts for each of the three steps of the overall reaction. For ethanol dehydrogenation we use nanocrystalline SnO_2, for the reforming step we use Co(Fe)/ZnO doped with Na^+, and for the final water gas shift step we use a commercial catalyst based on Fe_2O_3–Cr_2O_3. We first carry out detailed kinetic experiments over well-defined samples for the first two stages of the process and we present fitted parameters for power-law type kinetic expressions to quantify the correspondent reaction rates. A dynamic mathematical model of the three-stage reformer is introduced as a tool for control-oriented devices design. Finally, introductory simulation results are presented in order to show the dynamic behavior of the system.

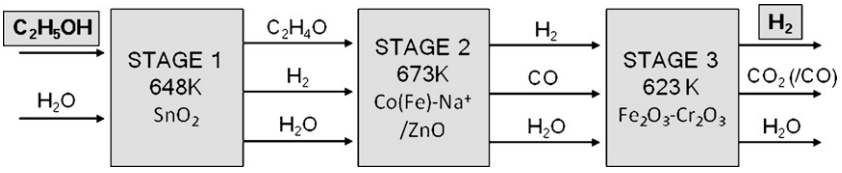

Fig. 1. Schematic representation of the three stage reforming process.

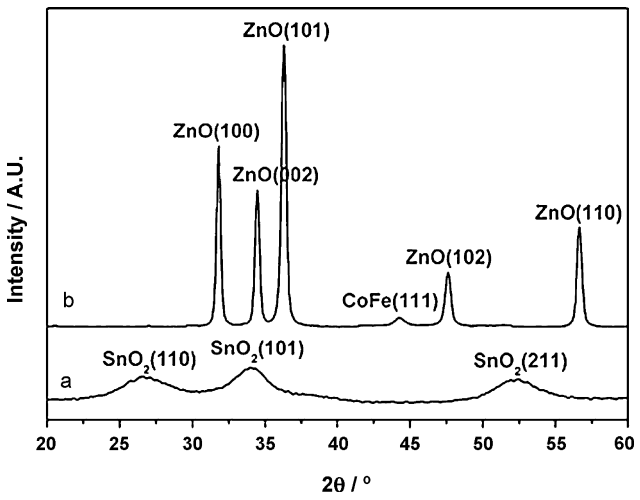

Fig. 2. X-ray diffraction profiles of catalysts SnO_2 (a) and Co(Fe)/ZnO (b).

2. Experimental

2.1. Catalysts preparation

SnO_2 was prepared by precipitation by the addition of ammonia to a $SnCl_4$ solution. The solid was aged for 2 h, dried at 303 K, and rinsed with distilled water repeatedly for chloride elimination. The resulting solid was dried at 373 K and treated at 573 K (0.5 K min^{-1}) for 6 h. Co(Fe)/ZnO catalyst with a cobalt content of 10% by weight, sodium content of 0.9% by weight, and Fe content of 1% by weight was prepared by co-precipitation at 313 K by the addition of a Na_2CO_3 solution to $Zn(NO_3)_2$, $Co(NO_3)_2$, and $Fe(NO_3)_2$ solutions. After aging at 313 K for 1.5 h, the suspension was filtered and the resulting solid washed with distilled water, dried at 363 K overnight, treated in air at 673 K (2 K min^{-1}) for 6 h, and reduced under hydrogen at 673 K (2 K min^{-1}) for 6 h.

2.2. Catalysts characterization

Chemical composition of catalysts was obtained by optical emission spectroscopy with inductively coupled plasma (ICP-OES, Perkin-Elmer Optima apparatus). BET surface area was determined using a Micromeritics ASAP 9000 apparatus. X-ray diffraction profiles (XRD) were collected at a step width of 0.02° and by counting 10 s at each step with a Siemens D-500 instrument equipped with a Cu target and a graphite monochromator. High-resolution transmission electron microscopy (HRTEM) was performed with a JEOL JEM 2010F electron microscope equipped with a field emission gun electron source operated at 200 kV and an Energy Electron Loss Spectrometer (EELS). Photoelectron spectra (XPS) were acquired with a Perkin-Elmer PHI-5500 spectrometer equipped with an Al X-ray exciting source and a hemispherical electron analyzer.

2.3. Catalytic tests

All the kinetic experiments were carried out at atmospheric pressure in a tubular reactor placed inside a temperature-controlled heating furnace. Experiments were conducted in the 573–673 K temperature range. An ethanol–steam mixture (C_2H_5OH:H_2O = 1:6, molar basis) or acetaldehyde–steam mixture (C_2H_4O:H_2O = 1:6, molar basis) was mixed with inert carrier gas and contacted with the catalyst inside the reactor. Products were analyzed on-line by gas chromatography and mass spectrometry. The reactor was brought to temperature under inert carrier gas flow before reaction. SnO_2 was used without any treatment, whereas the Co(Fe)/ZnO catalyst was treated inside the reactor under flowing, diluted H_2 (30 mL min^{-1}) at 673 K for 1 h prior to kinetic experiments. The weight of catalysts samples was varied in the range 0.03–0.1 g. The flow rates of ethanol and acetaldehyde were in the range 0.8–6.4 mL min^{-1}, while the total volumetric flow rate at reactor inlet, Q, was varied in the range 50–400 mL min^{-1}. Such diluted conditions assured a negligible volume change due to reaction. In addition, the volumetric flow rates were high enough to ensure the absence of external mass transfer limitations. In fact, an unaltered conversion level was measured when Q was increased while keeping constant the ratio between the weight of catalyst, W, and the molar flow rate of ethanol at reactor inlet (at constant temperature). Also, no pore diffusion resistance was encountered when varying catalyst particle size.

3. Catalytic and kinetic results

3.1. Ethanol dehydrogenation over SnO_2

The BET surface area of the SnO_2 catalyst was 120 m^2 g^{-1}. XRD and HRTEM showed that the catalyst is comprised exclusively by SnO_2 particles of about 5 nm. This is well exemplified in Fig. 2a, where X-ray diffraction lines are broad and correspond, according

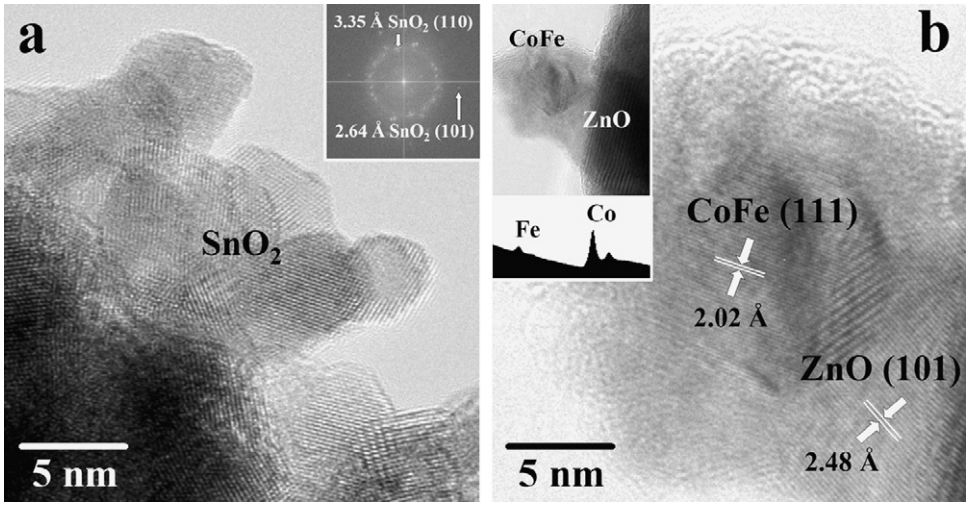

Fig. 3. High resolution transmission electron microscopy images of catalysts SnO_2 (a) and Co(Fe)/ZnO (b).

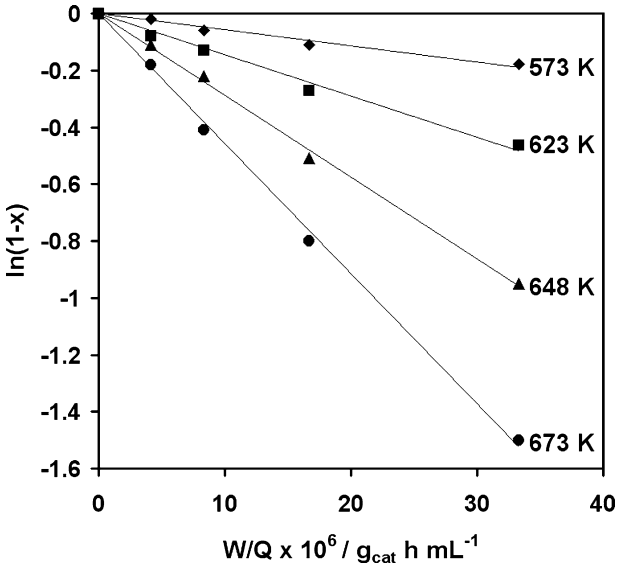

Fig. 4. Semilog plot of the mole fraction of unreacted ethanol as a function of W/Q at various temperatures over catalyst SnO_2.

to the Scherrer equation, to particles of 4.5 nm. Fig. 3a depicts a representative HRTEM image of this catalyst, showing particles in the range 4–6 nm, and its associated selected-area electron diffraction pattern with rings corresponding to multiple SnO_2 crystallites.

Under the temperature and W/Q conditions tested in this study, ethanol reacts over SnO_2 to yield exclusively acetaldehyde and hydrogen according to the reaction:

$$C_2H_5OH \rightarrow C_2H_4O + H_2 \quad (6)$$

In all cases, the yield of hydrogen approximately equals that of acetaldehyde as expected from the reaction stoichiometry ($[C_2H_4O]$:$[H_2]$ = 1:1). The order of the reaction was established by variation of the ethanol flow rate at a series of temperatures between 573 and 673 K. For a first-order reaction, the following relation holds true:

$$x = 1 - e^{-kW/Q} \quad (7)$$

where x is the degree of reactant conversion calculated on a molar basis as:

$$x = \frac{c_{in} - c_{out}}{c_{in}} \quad (8)$$

Eq. (7) can be rearranged as:

$$\ln(1-x) = -k\left(\frac{W}{Q}\right) \quad (9)$$

A plot of $\ln(1-x)$ vs. W/Q at various temperatures is shown in Fig. 4. As expected, for a given value of W/Q, the ethanol conversion increases with increasing temperature. It is also evident that the data at each temperature fall on a straight line. Therefore, the dehydrogenation reaction of ethanol is a first-order reaction and, according to Eq. (9), the slopes of the lines correspond to the specific reaction rate constant at the experimental temperatures. The values of k at the different temperatures tested along with the 95% confidence intervals are given in Table 1. A pre-exponential factor of 7.5×10^9 mL g_{cat}^{-1} h^{-1} is fitted from the data in Table 1 for an Arrhenius-type expression for the reaction rate constant (k). An Arrhenius plot of the rate constants exhibits good linearity, as depicted in Fig. 5. An activation energy of 66 ± 2 kJ mol^{-1} is obtained. The SnO_2 catalyst exhibited an excellent stability for ethanol dehydrogenation into acetaldehyde and hydrogen. A long-term run at 673 K and $W/Q = 33.3 \times 10^{-6}$ g_{cat} h mL^{-1} was conducted

Table 1
Values of the rate constant k at various temperatures in the dehydrogenation reaction of ethanol over SnO_2.

Temperature (K)	k (mL g_{cat}^{-1} h^{-1})	95% confidence interval
573	5.7×10^3	$\pm 0.2 \times 10^3$
623	1.5×10^4	$\pm 0.1 \times 10^4$
648	2.9×10^4	$\pm 0.3 \times 10^4$
673	4.6×10^4	$\pm 0.4 \times 10^4$

for 80 h and no deactivation in terms of ethanol transformation was observed.

3.2. Acetaldehyde reforming over Co(Fe)/ZnO

The Co(Fe)/ZnO catalyst contained well-dispersed, bimetallic Co–Fe nanoparticles over ZnO crystallites of about 40 nm. The BET surface area was 45 m^2 g^{-1}. The bimetallic nature of particles was evidenced by XRD and HRTEM techniques. Fig. 2b shows the XRD pattern of the catalyst where, in addition to narrow signals due to ZnO, a broad line at 44.8° corresponds to a Co–Fe alloy (pure Co (1 1 1) line is located at 51.8°). Fig. 3b shows a representative HRTEM image of the catalyst with a well-faceted Co–Fe particle. Lattice fringes at 2.02 Å correspond to the (1 1 1) plane of Co–Fe alloy. EELS recorded over single particles shows the presence of both Co and Fe, in accordance to the bimetallic nature of particles. Surface composition is Fe_{at}/Co_{at} = 0.2 and Na_{at}/Co_{at} = 1.0 as deduced from X-ray photoelectron spectroscopy.

The acetaldehyde-steam mixture was transformed over the Co(Fe)/ZnO catalyst into a mixture of hydrogen, carbon monoxide, and carbon dioxide under the experimental conditions used in this work. The selectivity towards methane was always maintained below 0.3% on a carbon basis. The distribution of products depended on temperature and W/Q. In particular, the higher the W/Q and the temperature, the higher the yield of hydrogen and CO_2. This is shown in Fig. 6 for the results obtained at 673 K. The effect of W/Q may be explained in terms of two consecutive reactions, namely the reforming of acetaldehyde into hydrogen and carbon monoxide (10), and the reaction of carbon monoxide with steam through the water gas shift reaction (3).

$$C_2H_4O + H_2O \rightarrow 2CO + 3H_2 \quad (10)$$

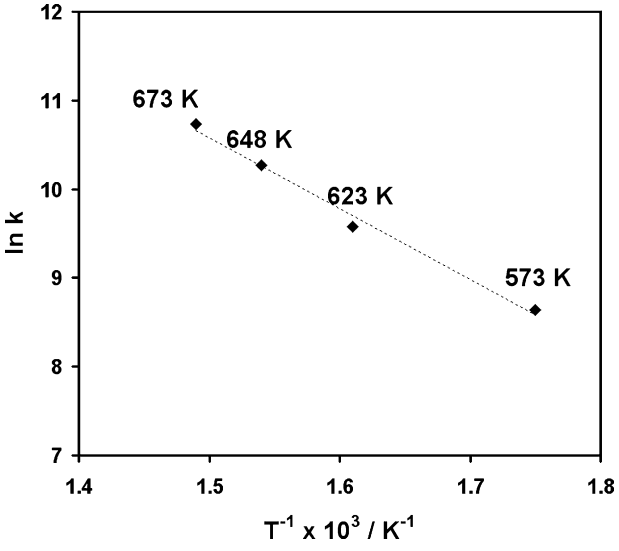

Fig. 5. Semilog plot of the specific reaction rates constants for the dehydrogenation of ethanol over catalyst SnO_2.

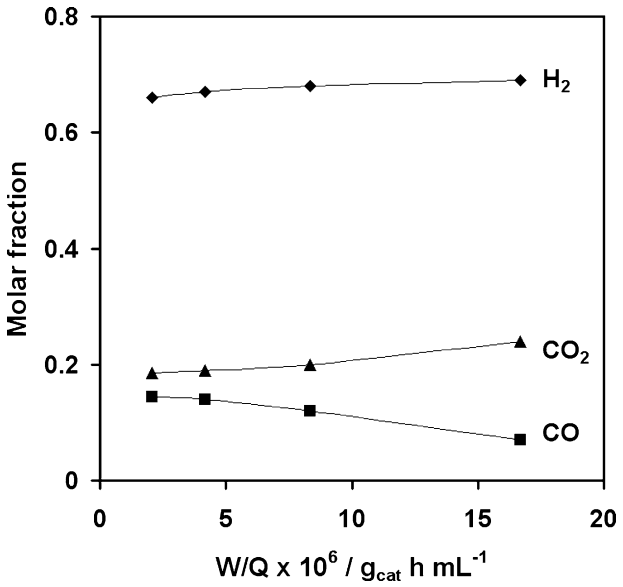

Fig. 6. Product distribution on a molar basis of carbon-containing products obtained in the acetaldehyde steam reforming reaction over catalyst Co(Fe)/ZnO at 673 K at different W/Q values.

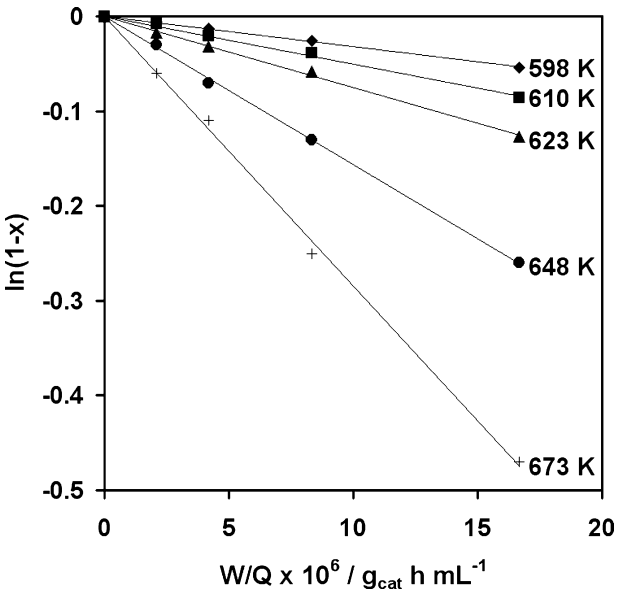

Fig. 8. Semilog plot of the mole fraction of unreacted acetaldehyde as a function of W/Q at various temperatures over catalyst Co(Fe)/ZnO.

The product distribution obtained in the experiments is in all cases in good agreement with the stoichiometry of reactions (10) and (3), and the equation:

$$C_{H_2} = C_{CO_2} + \frac{3}{2}(C_{CO} + C_{CO_2}) \quad (11)$$

at the reactor outlet holds true within the experimental error. The extent of the water gas shift reaction increases as W/Q increases due to a larger contact time between the reaction mixture and the catalyst. The increase of reaction temperature has also a positive effect on the water gas shift reaction in the temperature range used in this work. This is illustrated in Fig. 7, where the molar ratio between CO_2 and CO is plotted against W/Q at different temperatures. The maximum H_2 yield and CO_2/CO ratio is encountered at 673 K and 16.7×10^{-6} g_{cat} h mL^{-1}.

Concerning the kinetics of acetaldehyde steam reforming over the Co(Fe)/ZnO catalyst, Fig. 8 shows a plot of the log of residual acetaldehyde vs. W/Q at different temperatures between 598 and 673 K. It is found that the data at each temperature fall on a straight line. This, Eq. (9), means that the reaction is first order with respect to acetaldehyde. The first-order dependence on acetaldehyde is in agreement with results reported for other catalysts that have been studied for the ethanol reforming reaction, taking into account that the first step of the reaction is the dehydrogenation of ethanol into acetaldehyde, and that this first step is also a first order reaction. These other catalysts that have shown first-order dependence with respect to ethanol are Ru/Al_2O_3 [15], Ni/Al_2O_3, Ni/La_2O_3 and Ni/Y_2O_3 [16], and Cu plated Raney Ni [17].

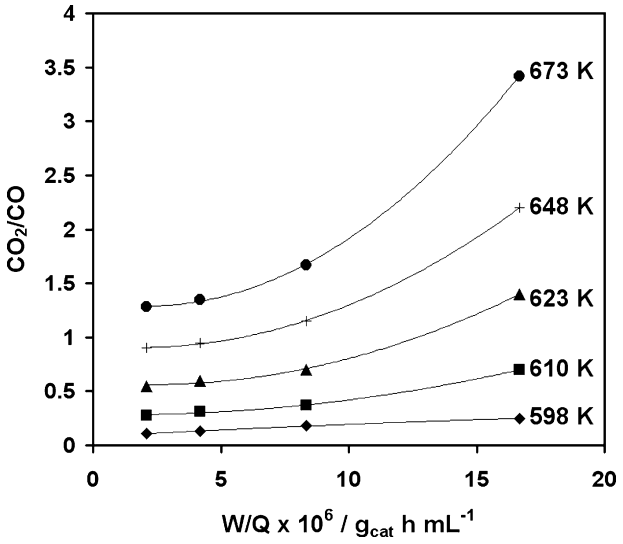

Fig. 7. Molar ratio between CO and CO_2 at different W/Q values and temperatures obtained after steam reforming of acetaldehyde over catalyst Co(Fe)/ZnO.

In all experiments performed over Co(Fe)/ZnO the steam-to-carbon ratio of S/C = 3 is much higher than that required from stoichiometry (Eq. (10)). The excess of water employed serves for preventing carbon deposition on the catalyst surface [4]. The slopes of the lines in Fig. 8 yield the apparent reaction rate constants at each temperature, k' (Eq. (10)). Table 2 compiles the values of k' at the different temperatures tested along with their 95% confidence intervals. A pre-exponential factor of 1.3×10^{12} mL g_{cat}^{-1} h^{-1} is fitted from the data in Table 2. An Arrhenius plot of the apparent rate constants is shown in Fig. 9. A good linearity is obtained and an activation energy value of 98 ± 4 kJ mol^{-1} is calculated. To our best knowledge, data regarding kinetic parameters for the ethanol steam reforming reaction over cobalt catalysts are scarcely found in the literature. Sahoo et al. [22] reports an activation energy of 83 kJ mol^{-1} for ethanol steam reforming over a Co/Al_2O_3 catalyst working at significantly higher temperatures (673–973 K). Therefore, the data presented here constitute a valuable reference for the reaction rate quantification over low-temperature cobalt ethanol reforming systems. Regarding the stability of the catalyst, it should be mentioned that a slow, but constant deactivation was observed during long-term runs at 673 K and $W/Q = 16.7 \times 10^{-6}$ g_{cat} h mL^{-1}

Table 2
Values of the apparent rate constant k' at various temperatures in the steam reforming reaction of acetaldehyde over Co(Fe)/ZnO.

Temperature (K)	k' (mL g_{cat}^{-1} h^{-1})	95% confidence interval
598	3.2×10^3	$\pm 0.1 \times 10^3$
610	5.0×10^3	$\pm 0.2 \times 10^3$
623	7.5×10^3	$\pm 0.3 \times 10^3$
648	1.6×10^4	$\pm 0.2 \times 10^4$
673	2.9×10^4	$\pm 0.4 \times 10^4$

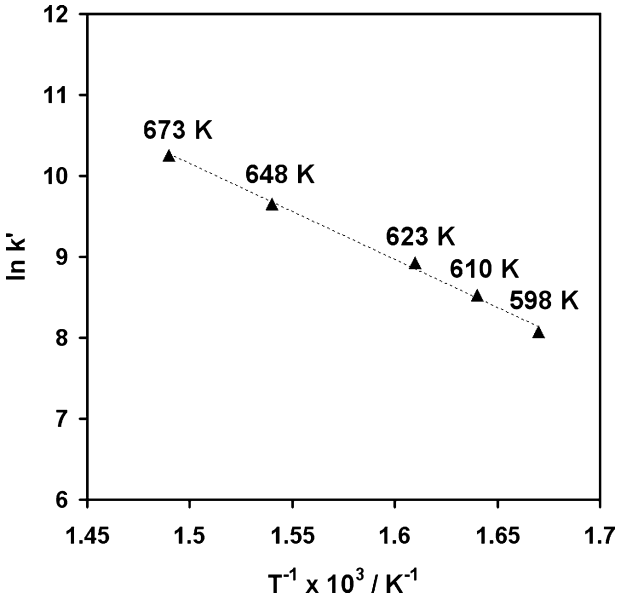

Fig. 9. Semilog plot of the specific reaction rates constants for the steam reforming of acetaldehyde over catalyst Co(Fe)/ZnO.

over the Co(Fe)/ZnO catalyst under acetaldehyde steam reforming. Acetaldehyde conversion decreased ca. 3% after continuous operation for 140 h, although no significant change of selectivity was observed.

3.3. Water gas shift reaction over Fe_2O_3–Cr_2O_3

From Figs. 7 and 8 it is deduced that the conversion of CO into CO_2 is not complete over the Co(Fe)/ZnO catalyst under the reaction conditions used in this work. To reduce the CO content of the stream leaving the reforming stage and to increase the hydrogen yield, a third stage is introduced, where the water gas shift reaction (WGSR, Eq. (3)) is performed. To shift the thermodynamic equilibrium towards H_2 and CO_2, this stage is operated at a lower temperature than the preceding stages (ethanol dehydrogenation into acetaldehyde and acetaldehyde reforming). The WGSR is an industrially important reaction and several commercial catalysts are available as well as numerous studies of its reaction kinetics. For modeling purposes, the present contribution considers the kinetics of the WGSR over a Fe_2O_3–Cr_2O_3 catalyst as reported by Podolski and Kim [18].

4. Dynamic modeling

4.1. Mathematical model

To perform the intended ethanol reforming process, three monolithic reactors in series are selected (see Fig. 1). The reactors should provide the necessary hydrogen flow for the operation of a fuel-cell system for electric power generation. An accurate knowledge of the dynamic response of the reactors results essential towards the design of the control system of the whole unit, which should consider also the restrictions imposed by the fuel cell. The operation with chemical reactors usually implies difficulties in control issues due to the delays in response, the high sensibility to the operation temperature and the difficulty of obtaining intermediate measurements. Therefore, the development of a dynamic model of the reactor is an indispensable tool for the development of the controllers.

A one-dimensional, pseudo-homogeneous, non-steady-state model has been used to represent the ethanol reforming in the already referenced series of monolithic reactors. Pseudo-homogeneous mathematical models are usually selected for control-oriented applications to reduce the solving time of the equations system. Each of the first two monolithic sections is modeled with the catalysts data described in Section 3, the third unit is provided with a standard formulation for the water gas shift reaction [18]. For simplicity, no CO_2 formation is considered in stage 2 of the model. Thermally isolated lines are considered between sections. The use of low-diameter monoliths and optimized inlet distributors supports the assumption of 1D model avoiding the occurrence of pronounced radial mass and temperature profiles. The outlet wall of the monolithic reactors are assumed at constant temperature (the reaction units are placed into a furnace), although different temperature levels are considered for the different stages. The pressure drop in the reactors was assumed negligible due to the high void fractions of monolithic structures [19,20]. The mass and energy balances used to represent the non-steady-state reactor behavior, along with the corresponding initial and boundary conditions, are presented below:

Mass balance (component j):

$$\frac{\partial C_j}{\partial t} + \frac{\partial (v C_j)}{\partial z} = \upsilon_{j,i} r_i \tag{12}$$

Energy balance:

$$\left[\rho_g c_{p_g} + \rho_s c_{p_s}\right] \frac{\partial T}{\partial t} + \rho_g c_{p_g} v \frac{\partial T}{\partial z} = \frac{4U}{d_t} (T_F - T) + (-\Delta H_i) r_i \tag{13}$$

The numerical solution of the set of partial differential equations (12) and (13) was accomplished by its transformation into an ODE-system by discretization of the spatial derivative. To this end, backward finite differences have been selected (first-order, 90 discretization points for the reported simulations). The resultant ODE equations were solved by an algorithm implemented in MATLAB™ (ODE45 Normand-Prince). The ideal gas assumption is considered due to the low operating pressure of ca. 1 bar. Values of the specific heat for each component and of the gas mixture are taken from Perry and Chilton [21]. A bulk void fraction of $\varepsilon = 0.66$ is consequent with the modeled monolithic reactors. A catalyst loading of 0.15 $kg_{cat}\ kg_s^{-1}$ and a total solid density of $\rho_s = 500\ kg_s\ m_R^{-3}$ are considered for modeling purposes. An arbitrary constant value for the overall-heat-transfer coefficient (U) of 100 $W\ m^{-2}\ K^{-1}$ was selected for these introductory simulations.

4.2. Simulations

The stages of the proposed ethanol reforming system were dimensioned to provide the necessary hydrogen flow to feed a 1 kW fuel cell (efficiency = 0.5) of a low-scale autonomous power production device. Conversions of ethanol, acetaldehyde and carbon monoxide higher than 90% are required. Reactor volumes of 1.2, 1.6 and 1.2 L result from these requirements for a total input molar flow of 10 mmol s^{-1}, an ethanol–water molar ratio of 1:6, inlet temperature of the feed of 648 K and operating temperatures for the furnaces of each stage of 648, 673 and 633 K, respectively. Assuming a maximum monolith diameter of 0.02 m, a multitubular configuration for the different stages would be required to lead to a feasible design.

Steady-state molar fraction axial profiles are presented in Figs. 10–12 for stages 1–3, respectively. Conversions of ethanol, acetaldehyde and carbon monoxide of 94, 91 and 92% are achieved for stages 1–3, respectively. Heat flows of +86 and +233 W are required for stages 1 and 2, while stage 3 delivers −92 W, resulting in a heat requirement of +227 W for the whole unit. This value represents ca. 13% of the LHV of the hydrogen provided by the system. An exit CO molar fraction (stage 3, see Fig. 1) of ca. 0.012 points out the need of a final purification step facing the PEMFC feeding.

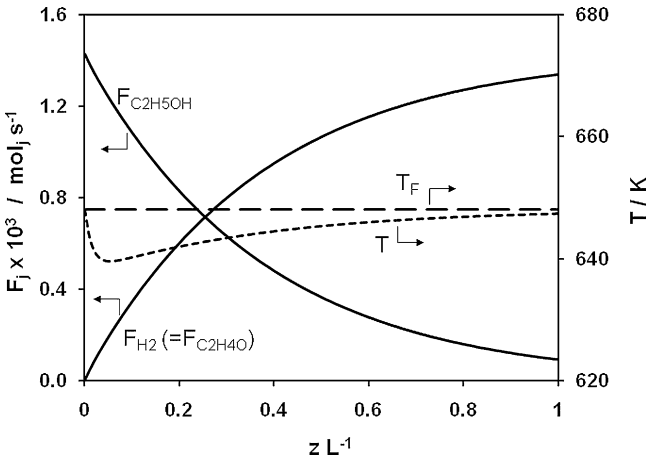

Fig. 10. Stage 1, temperature and molar flow axial profiles. Steady state, $T_{in} = 648$ K, $T_F = 648$ K, $F_{T,in} = 0.0095$ mol s^{-1}, $y_{C_2H_5OH,in} = 0.143$, $d_t = 0.02$ m, and $L = 4$ m.

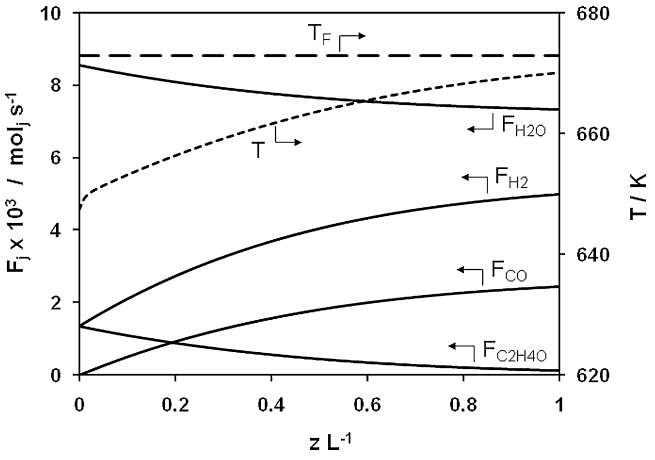

Fig. 11. Stage 2, temperature and molar flow axial profiles. Steady state, $T_F = 673$ K, $d_t = 0.02$ m, and $L = 5$ m.

Maximum differences between process and furnace temperatures of ca. −10, −25 and +45 K are observed.

To show the dynamic response of the reforming unit, Figs. 13–15 present concentration temporal profiles at the exit of the three reactor zones after disturbing the input flow, and assuming a constant value for the volumetric flowrate. Specifically, step-like perturbations in ethanol and water inlet concentrations (+10% during 5 s) are performed at $t = 10$ s and $t = 50$ s, respectively. Temperature disturbances (of the feed and furnace temperatures of the three stages) were also applied in the simulated system and a sensitivity anal-

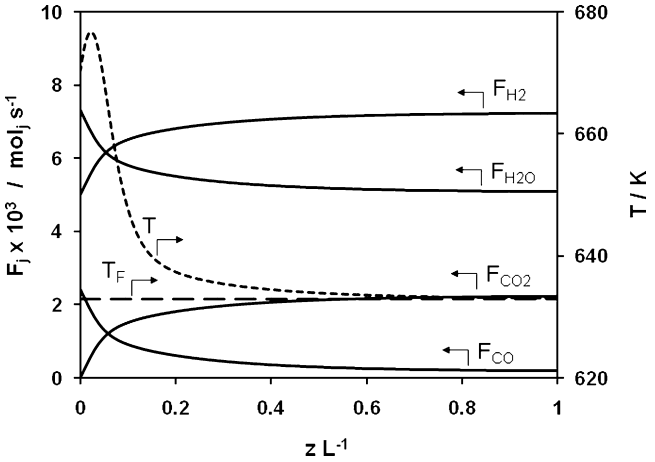

Fig. 12. Stage 3, temperature and molar flow axial profiles. Steady state, $T_F = 633$ K, $d_t = 0.02$ m, and $L = 3.7$ m.

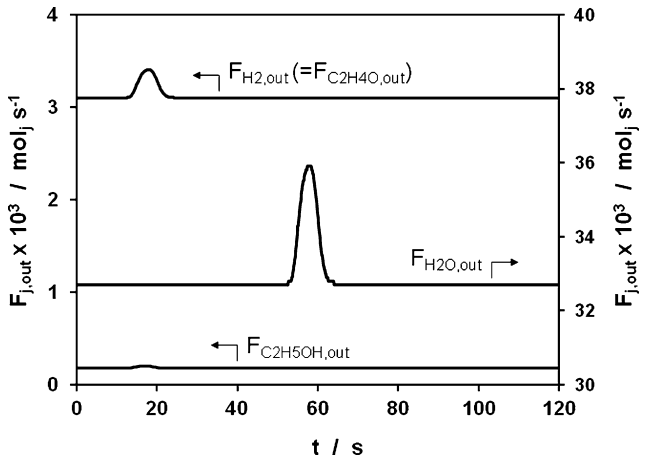

Fig. 13. Stage 1, dynamic response of the exit molar flows ($z = L$) for a step-like perturbation of +10% in the ethanol inlet concentration between 10 and 15 s and +10% in the water inlet concentration between 50 and 55 s. $F_{T,in} = 0.036$ mol s^{-1}, $y_{C_2H_5OH,in}$: $y_{H_2O,in} = 1 : 10$, isothermal operation at $T_F = 648$ K, $d_t = 0.06$ m, and $L = 1.45$ m.

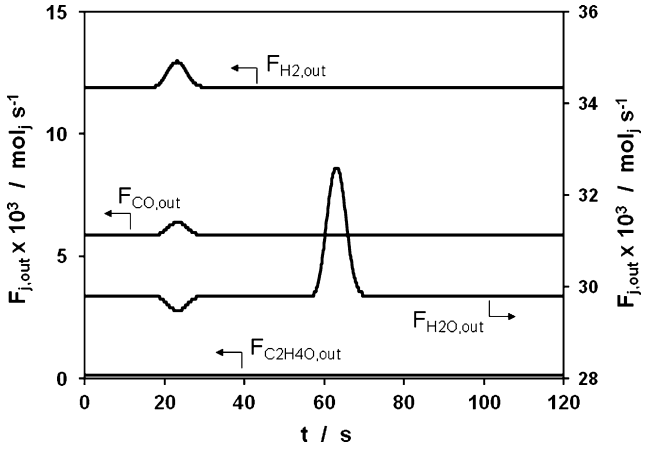

Fig. 14. Stage 2, dynamic response of the exit molar flows ($z = L$). Perturbation as in caption of Fig. 13. Isothermal operation at $T_F = 673$ K, $d_t = 0.06$ m, and $L = 1.56$ m.

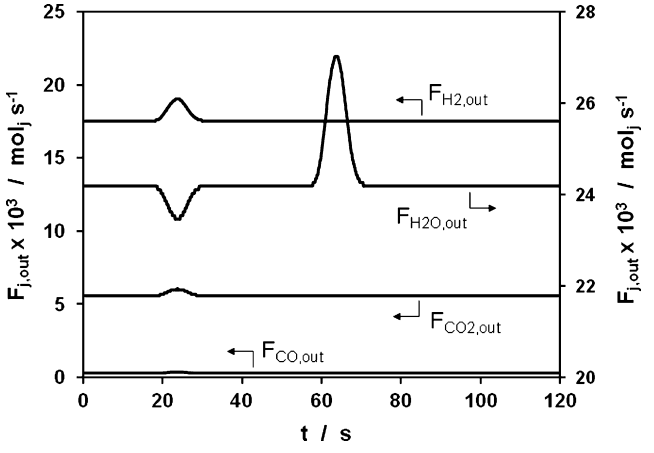

Fig. 15. Stage 3, dynamic response of the exit molar flows ($z = L$). Perturbation as in caption of Fig. 13. Isothermal operation at $T_F = 633$ K, $d_t = 0.06$ m, and $L = 0.16$ m.

ysis is currently being done. The pure delay of approximately 11 s observed in the dynamic response (Figs. 13–15), and the sensibility of the hydrogen production to the operating conditions of the feed will be critical points for the design of controllers for fuel cells with changeable load.

5. Conclusions

The present work addresses the low-temperature ethanol steam reforming for hydrogen production for fuel cell feeding. The proposed unit comprises three reactors in series and profits from the well-known ability of Co-based catalysts for performing the reforming reaction at moderate temperatures. The intended system clearly fits the requirements of a low-scale autonomous power production facility. The three stages of the proposed design correspond to ethanol dehydrogenation over SnO_2, acetaldehyde reforming over Co(Fe)/ZnO, and water gas shift reaction over commercial Fe_2O_3–Cr_2O_3. Kinetic parameters have been obtained in various sets of experiments, which have been used for the design of up-scaled monolithic reactors. A non-steady-state mathematical model has been developed and used to simulate the dynamic response of the reforming unit for disturbances in the input variables. A response delay of ca. 11 s has been obtained, which will have important implications in the design of the automatic control device for an integrated reformer and fuel cell system.

Acknowledgements

This research was supported by projects MEC ENE2006-06925 and CICYT DPI2007-626966.

References

[1] P.D. Vaidya, A.E. Rodrigues, Chem. Eng. J. 117 (2006) 39–49.
[2] A. Haryanto, S. Fernando, N. Murali, S. Adhikari, Energy Fuels 19 (2005) 2098–2106.
[3] J. Llorca, N. Homs, J. Sales, P. Ramírez de la Piscina, J. Catal. 209 (2002) 306–317.
[4] J. Llorca, P. Ramírez de la Piscina, J.A. Dalmon, J. Sales, N. Homs, Appl. Catal. B: Environ. 43 (2003) 355–369.
[5] A. Casanovas, M. Saint-Gerons, F. Griffon, J. Llorca, Int. J. Hydrogen Energy 33 (2008) 1827–1833.
[6] J. Llorca, A. Casanovas, T. Trifonov, A. Rodríguez, R. Alcubilla, J. Catal. 255 (2008) 228–233.
[7] J.A. Torres, J. Llorca, A. Casanovas, M. Domínguez, J. Salvadó, D. Montané, J. Power Sources 169 (2007) 158–166.
[8] S. Cavallaro, N. Mondello, S. Freni, J. Power Sources (2001) 198–204.
[9] J. Llorca, P. Ramírez de la Piscina, J. Sales, N. Homs, Chem. Commun. (2001) 641–642.
[10] S.C. Lyu, T.J. Lee, C.W. Yang, C.J. Lee, Chem. Commun. (2003) 1404–1405.
[11] J. Llorca, N. Homs, J. Sales, J.L.G. Fierro, P. Ramírez de la Piscina, J. Catal. 222 (2004) 470–480.
[12] J. Llorca, N. Homs, P. Ramírez de la Piscina, J. Catal. 227 (2004) 556–560.
[13] J. Llorca, J.A. Dalmon, P. Ramírez de la Piscina, N. Homs, Appl. Catal. A: Gen. 243 (2003) 261–269.
[14] J. Llorca, P. Ramírez de la Piscina, J.A. Dalmon, N. Homs, Chem. Mater. 16 (2004) 3573–3578.
[15] P.D. Vaidya, A.E. Rodrigues, Ind. Eng. Chem. Res. 45 (2006) 6614–6618.
[16] J. Sun, X.-P. Qiu, F. Wu, W.-T. Zhu, Int. J. Hydrogen Energy 30 (2005) 437–445.
[17] D.A. Morgenstern, J.P. Fornango, Energy Fuels 19 (2005) 1708–1716.
[18] W.F. Podolski, Y.G. Kim, Ind. Eng. Chem. 13 (1974) 415–421.
[19] S. Irandoust, B. Andersson, Catal. Rev. Sci. Eng. 30 (3) (1988) 343–391.
[20] A. Cybulski, J.A. Moulijn, Catal. Rev. Sci. Eng. 36 (2) (1994) 179–269.
[21] R.H. Perry, C.H. Chilton, Manual del Ingeniero Químico, McGraw-Hill, Bogotá, 1982.
[22] D.R. Sahoo, S. Vajpai, S. Patel, K.K. Pant, Chem. Eng. J. 125 (3) (2007) 139–147.